Bright Luminescence from Non-toxic $CsCu_2X_3$ (X = Cl, Br, I)

Rachel Roccanova,[1‡] Aymen Yangui,[1‡] Gijun Seo,[2] Tielyr D. Creason,[1] Yuntao Wu,[3,4] Do Young Kim,[2] Mao-Hua Du,[5] Bayrammurad Saparov[1*]

[1]Department of Chemistry and Biochemistry, University of Oklahoma, 101 Stephenson Parkway, Norman, OK 73019, USA

[2]School of Materials Science and Engineering, Oklahoma State University-Tulsa, 526 N. Elgin Ave, Tulsa, OK 74106, USA

[3]Synthetic Crystal Research Center, Shanghai Institute of Ceramics, Chinese Academy of Sciences, Shanghai, 201800, China

[4]Scintillation Materials Research Center and Department of Materials Science and Engineering, University of Tennessee, Knoxville, Tennessee, 37996, USA

[5]Materials Science and Technology Division, Oak Ridge National Laboratory, Oak Ridge, TN 37831, USA

[*]E-mail: saparov@ou.edu

[‡]These authors contributed equally to this work

ABSTRACT. Inexpensive and highly-efficient luminescent materials based on multinary halides have received increased attention in recent years. Among those considered most promising are the perovskites such as $CsPbX_3$ due to their highly efficient and tunable emission through precise control of chemical composition and nanostructuring. However, the presence of the toxic heavy metal Pb and relatively poor stability are among the major challenges for the introduction of lead halide-based materials into the marketplace. Here, we report the optical properties of nontoxic and highly emissive one-dimensional (1D) all-inorganic halides $CsCu_2X_3$ (X = Cl, Br, I) and their mixed halide derivatives, which also show improved thermal and air stability. Photoluminescence (PL) measurements show a tunable bright room temperature emission from green to yellow with photoluminescence quantum yields ranging from 0.38% ($CsCu_2Br_{1.5}I_{1.5}$) to 48.0% ($CsCu_2Cl_3$). Temperature and power-dependent PL measurements suggest that the emission results from self-trapped excitons induced by strong charge localization and structural distortions within the lD ribbon structure.

TOC GRAPHIC

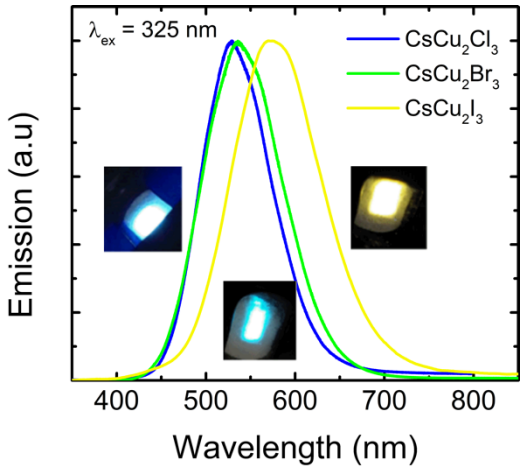

Halide perovskites have emerged as promising materials for optoelectronics[1-2] due to their outstanding photovoltaic and tunable light emission properties that results from the vast variability of their compositions and dimensionalities.[3-4] This has been observed in several all-inorganic and hybrid organic-inorganic halide systems such as the three dimensional (3D) perovskite $CsPbX_3$[5] where varying the halide composition,[6] crystal size,[7] and dimensionality impacts the emission color and efficiency. Moreover, lowering the structural dimensionality from 3D down to zero dimensional (0D) leads to quantum confinement effects, which yield exceptionally high exciton binding energies,[8] such as in the case of $CsPbX_3$ nanocrystals and Cs_4PbX_6. Indeed, the presence of room temperature (RT) stable excitons in low-dimensional halide systems has proven advantageous for enhanced RT luminescence properties observed for a number of materials including the green-emitting Cs_4PbBr_6,[10] $CsCuBr_2$,[11] Cs_2CuCl_4,[12] which shows a largely Stokes-shifted broad-band green emission from copper defects, and the blue-emitting $Cs_3Cu_2Br_{5-x}I_x$,[13] which all exhibit low-dimensional (0-2D) crystal structures. Therefore, the emission properties of such halides are being considered for light-emitting diodes (LEDs) which are actively pursued as a part of the global effort to implement the energy-efficient solid-state lighting technologies.[14]

Here, we report the photophysical properties of earth-abundant and non-toxic $CsCu_2X_3$ (X = Cl, Br, I) family that exhibits high efficiency light emission properties with photoluminescence quantum yield (PLQY) values up to 48%. $CsCu_2X_3$ (X = Cl, Br, I) crystallize in the orthorhombic space group *Cmcm* in a 1D ribbon-like crystal structure (Figure 1),[15-16] featuring edge-sharing $[Cu_2X_3]^-$ anionic ribbons separated by rows of Cs^+ atoms. The high PLQYs of $CsCu_2X_3$ is thus attributed to the 1D chain structure in this family. A more in-depth structural analysis can be found in the supporting information (SI). Some members of this family have proven to be solution-processable, however, suitable samples of $CsCu_2X_3$ for optical characterization could only be

formed through solid-state synthesis. Purity of all samples were assessed with powder X-ray diffraction (PXRD) measurements, (Figures S1-S2), confirming that the crystallographic parameters increase linearly as the size of the halide increases following Vegard's law (Figure S3 and Tables S1-2), which is also common for other compounds in this ternary system[13] and Pb-based halides such as $FA_{1-x}Cs_xPbBr_3$.[17]

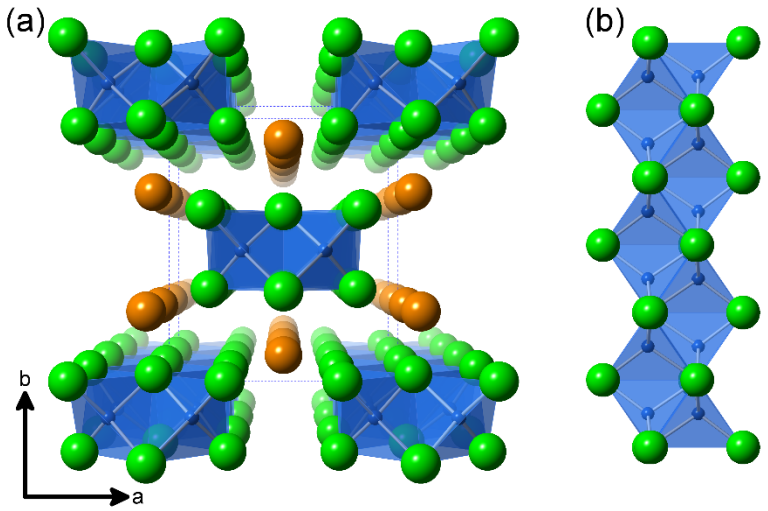

Figure 1. (a) The one-dimensional (1D) crystal structure of $CsCu_2X_3$ (X = Cl, Br, I) projected along the *c*-axis. Orange, blue and green spheres represent Cs, Cu and X, respectively. (b) A close-up view of the polyanionic $[Cu_2X_3]^-$ chain formed through edge-sharing connectivity of CuX_4 tetrahedra.[15-16]

The stability of a material in ambient air/moisture and over a large range of temperatures is highly important for optoelectronic device applications. Based on periodic PXRD and the simultaneous measurements of thermogravimetry (TGA) and differential scanning calorimetry (DSC), $CsCu_2X_3$ show good ambient air stability for more than two months (Figure S4), and an excellent thermal stability up to 495 °C with minimal mass loss after two heating-cooling cycles (Figure S5), which is a notable improvement over other well-known metal halides such as $(CH_3NH_3)PbI_3$ and $(CH_3NH_3)_3Bi_2I_9$.[18] Moreover, $CsCu_2X_3$ family members exhibit congruent melting behavior, with melting occurring at 270 °C, 351 °C and 374 °C for $CsCu_2Cl_3$, $CsCu_2Br_3$

and $CsCu_2I_3$, respectively.[19-20] In addition, the presence of a small peak feature in each sample close to their melting transitions suggests the presence of a minor CsX impurity. Indeed, CsX impurities are known to form a lower melting eutectic together with $CsCu_2X_3$.[19-20] Finally, photosensitivity of $CsCu_2X_3$ was checked through periodic measurements of PLQY under continuous irradiation at their respective PLE_{max}, which showed up to 10% loss in PLQY for the chloride and no change in bromide and iodide samples.

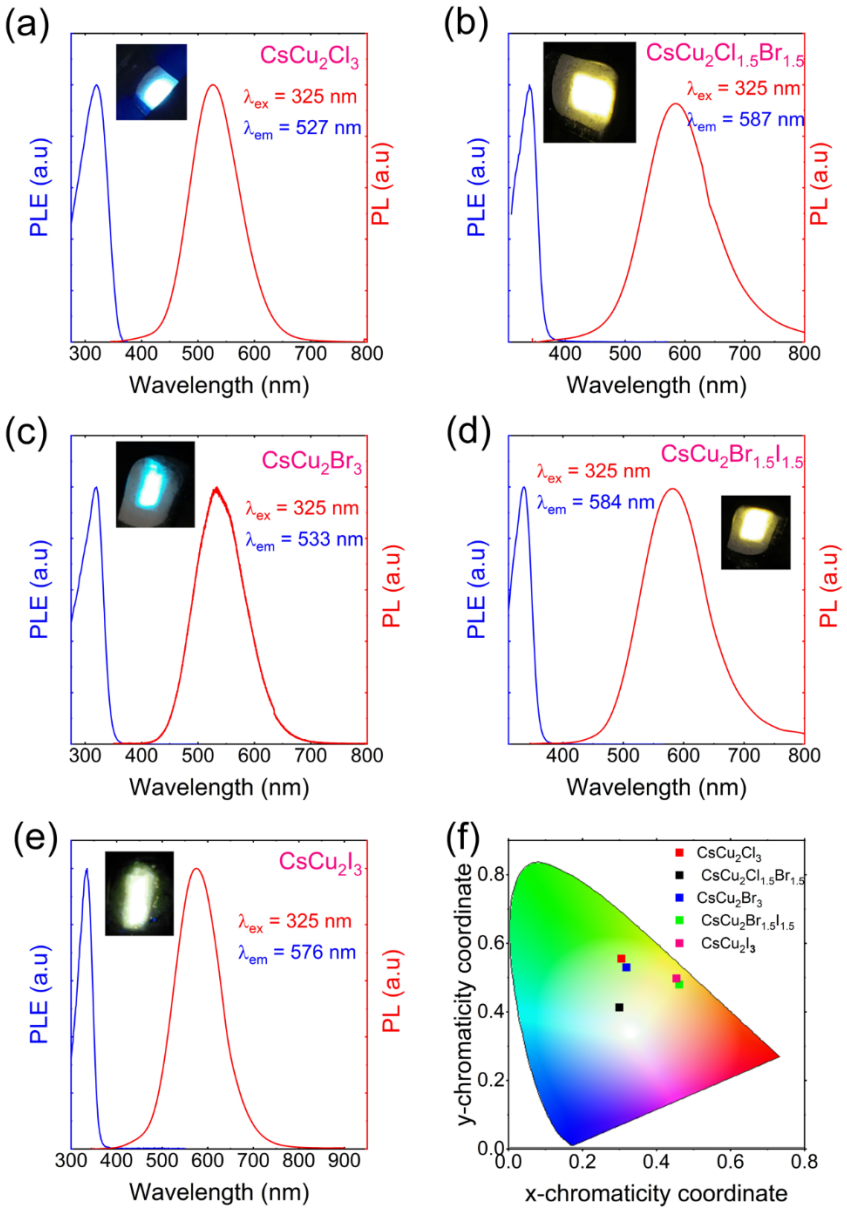

Figure 2. Photoluminescence excitation (blue) and emission (red) for (a) $CsCu_2Cl_3$, (b) $CsCu_2Cl_{1.5}Br_{1.5}$, (c) $CsCu_2Br_3$, (d) $CsCu_2Br_{1.5}I_{1.5}$, and (e) $CsCu_2I_3$. (d) A CIE 1931 plot with the emission colors of $CsCu_2X_3$.

On the basis of the Kubelka-Munk plots, shown in Figure S6, halide substitution leads to tunable band gaps energies, ranging from 3.74 to 3.53 eV. The density functional theory (DFT) calculation based on the PBE functional shows direct band gaps for $CsCu_2Cl_3$, $CsCu_2Br_3$, and $CsCu_2I_3$. The valence (conduction) band is made up of Cu-3d (Cu-4s) orbitals hybridized with halogen-p orbitals. The PBE band structure and density of states of $CsCu_2Cl_3$, which was chosen as a representative of the family, are shown in Figure S7. Note that the PBE band gap is underestimated due to the well-known band-gap error in the PBE calculation. We further corrected the band gap using the hybrid PBE0 functional. The PBE0 band gaps of $CsCu_2Cl_3$, $CsCu_2Br_3$, and $CsCu_2I_3$ are 4.29 eV, 3.94 eV, and 3.93 eV, respectively. The calculated band gaps are higher than the measured PLE energies because the calculation does not take into account the exciton binding; however, the calculated band gap trend is consistent with that of the measured PLE energies.

Under 325 nm UV excitation at RT, $CsCu_2X_3$ show highly Stokes-shifted emission from 527 to 587 nm with PLQYs values ranging from 0.38% ($CsCu_2Br_{1.5}I_{1.5}$) to 48.0% ($CsCu_2Cl_3$) and CIE 1931 chromaticity coordinates of (0.31, 0.55), (0.32, 0.53), and (0.46, 0.50) for $CsCu_2Cl_3$, $CsCu_2Br_3$, and $CsCu_2Cl_3$, respectively (Table 1 and Figure 2). The observed bright RT emission result from strong quantum confinement and highly localized charges promoting a high exciton binding energy (few hundreds of meV, see below)[21] and yielding high PLQY, which are often observed in low-dimensional metal halides.[8, 13, 22-23] The excitation spectra (PLE) contain excitation peaks ranging from 319 nm for $CsCu_2Cl_3$ to 340 nm for $CsCu_2Cl_{1.5}Br_{1.5}$ (Table 1 and Figure 2). Normalized PLE spectra measured for different emission wavelengths have identical shape and features, suggesting that the emission in $CsCu_2X_3$ have the same physical origin (Figure

S8). The recorded Stokes shift and full width at half maximum (FWHM) show an increasing trend going from the chloride to the iodide member. In semiconductors, the presence of permanent defect states can create broadband emission.[24] However, our power dependence PL measurements (Figure S9) show linear behavior for all studied compounds and the absence of saturation excludes the possibility of permanent defect emission.[25-26] Therefore, we attribute the largely Stokes-shifted broadband emission of $CsCu_2X_3$ to self-trapped excitons (STEs). It is worth noticing that the maximum PL of the single halides (X = Cl, Br, I) shows a continuous red-shifts corroborated with an increase of the Stokes shifts, however, the mixed halides $CsCu_2Cl_{1.5}Br_{1.5}$ and $CsCu_2Br_{1.5}I_{1.5}$ do not follow a linear trend and their maximum emission are red-shifted and lower in efficiency compared to the single halides (see Table 1). A similar behavior was also observed for $MAPb(IBr)_3$.[27] These facts could be explained by the presence of more structural distortion in the mixed halide samples, which can affect the PL efficiency, the self-trapping depth within the band gap of the material and lead to a red shift of the maximum PL.[28]

Table 1. Photoluminescence information table for all members.

Compound	PLQY (%)	FWHM (nm)	PLE (nm)	PL (nm)	CIE coordinates	CCT (K)	Stokes-shift (nm)	Lifetime (ns)
$CsCu_2Cl_3$	48.0	102	319	527	(0.29, 0.52)	6437	208	13.8
$CsCu_2Cl_{1.5}Br_{1.5}$	0.37	200	340	587	(0.089, 0.52)	12577	247	15.1
$CsCu_2Br_3$	18.3	106	319	533	(0.27, 0.53)	6872	214	18
$CsCu_2Br_{1.5}I_{1.5}$	0.38	128	335	584	(0.48, 0.51)	3094	249	26.6
$CsCu_2I_3$	3.23	126	334	576	(0.43, 0.47)	3561	242	62

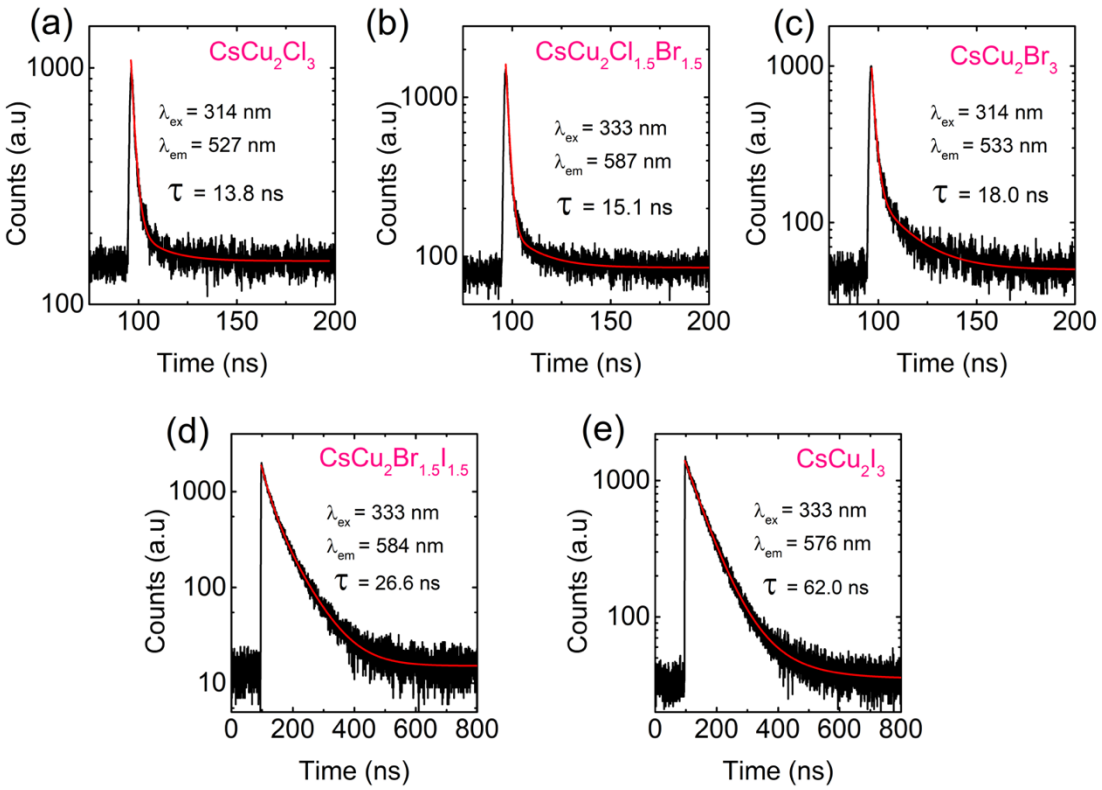

Figure 3. Room temperature time-resolved PL of (a) $CsCu_2Cl_3$, (b) $CsCu_2Cl_{1.5}Br_{1.5}$, (c) $CsCu_2Br_3$, (d) $CsCu_2Br_{1.5}I_{1.5}$, (e) $CsCu_2I_3$.

Figure 3 shows the RT time-resolved photoluminescence (TRPL) measurements of $CsCu_2X_3$. All decay profiles can be fitted using the two-exponential function,

$$I(t) = A_1 \times \exp\left(\frac{-t}{\tau_1}\right) + A_2 \times \exp\left(\frac{-t}{\tau_2}\right) + I_0 \qquad (1)$$

The full refinement results are provided in Table S4 in the SI. Excitons lifetimes vary between 13.8 and 62.0 ns, and show an increase going from Cl, Br, to I, which is in agreement with those of homologous compounds such as $CsPbBr_3$[29] and inversely proportional to the measured PLQYs (48% for the Cl-, 18.3% for the Br-, and 3.23% for the I-based compounds). Note that STEs lifetime was discussed by Mott and Stoneham based on the consideration of an energy barrier that is required to be surmounted for STEs formation.[30] The potential barrier between STEs and free-

excitons should be higher for $CsCu_2I_3$ compared to $CsCu_2Cl_3$, which explain the longer relaxation time for excitons in $CsCu_2I_3$ compared to $CsCu_2Br_3$ and $CsCu_2Cl_3$.

To get further information about the STEs dynamics and the exciton-phonon interaction, we measured the temperature dependence of PL for $CsCu_2X_3$ under 325 nm excitation (Figures 4a and S10, Table S5). The PL intensity of $CsCu_2Cl_3$ shows a relatively small thermal quenching (~ 3 times) upon heating. However, the thermal quenching is much more significant for $CsCu_2I_3$ (~ 5 times) and the alloyed $CsCu_2Br_{1.5}I_{1.5}$ (~ 60 times). This is consistent with the trend of the measured PLQYs values (Table 1) and confirms that excitons are more thermally stable in $CsCu_2Cl_3$. Based on the temperature-dependent PL data, we studied the thermal evolution of the integrated intensity, the position, and FWHM of PL peaks of $CsCu_2X_3$ (Figure 4b-d). In semiconductors, free exciton PL peak red-shifts upon heating following Varshni's model.[31] Here, the position of PL peaks of $CsCu_2X_3$ slightly blue-shit upon heating, particularly for $CsCu_2I_3$ (Figure 4b). Such a blue-shift was also observed in some metal halides[32-33] and PbS quantum dots,[34] and was attributed to the strong electron-phonon coupling. This is also consistent with the high lattice distortion of $CsCu_2I_3$ (Table S3). Moreover, for non-alloy compounds $CsCu_2Cl_3$, $CsCu_2Br_3$ and $CsCu_2I_3$, the integrated PL intensity quenches upon cooling and then saturate 100 K (Figure 4c). This thermal quenching can be described by the Arrhenius-type model,[35]

$$I_{PL} = \frac{I_0}{(1 + a \times exp(\frac{-E_b}{k_B T}))}, \quad (2)$$

where I_0 is the low-temperature PL intensity, k_B is the Boltzmann constant, a is the ratio between the radiative and the nonradiative decay rates, and E_b is the exciton binding energy. The best fit gives E_b of 201 ± 6, 155 ± 4, and 128 ± 1, for $CsCu_2Cl_3$, $CsCu_2Br_3$ and $CsCu_2I_3$, respectively. These high E_b values are much larger than that of the 3D perovskite $CsPbX_3$ (~18 meV),[36] characteristic of low-dimensional materials as discussed earlier. Importantly, the trend of the

exciton binding energy furthermore support the increasing of the PLQYs values from 3.23 for $CsCu_2I_3$ to 48% for $CsCu_2Cl_3$.[37-39] On the other hand, the integrated PL intensity of the alloys compounds $CsCu_2Cl_{1.5}Br_{1.5}$ and $CsCu_2Br_{1.5}I_{1.5}$, first increases with temperature from 4 to 80 K, then decreases at higher temperature (Figure 4c). The initial increase of PL intensity with temperature, known as "negative thermal quenching",[40] was already observed in semiconductors,[41] and metal halides,[42] and attributed to phonon-assisted nonradiative recombination. These data can be refined using the Shibata model,[40] which involves two competing processes: the quenching of the PL intensity with temperature due to thermal dissociation of the electron-hole pair and the subsequent decrease of the exciton population, and negative thermal quenching due to the thermal excitation of low-energy nonradiative STEs states towards the higher energy radiative STEs state responsible for the quenching of the PL of the two alloys compounds $CsCu_2Br_{1.5}I_{1.5}$ and $CsCu_2Br_{1.5}I_{1.5}$. In addition, detrapping of excitons, from STEs to free excitons states, may also lead to thermal quenching of the PL emission.[43] Therefore, we consider two activation energies for the thermal quenching process, and the temperature dependence PL intensity is given by,

$$I(T) = I_0 \frac{1 + c \times exp^{(-E_c/k_B T)}}{1 + a \times exp^{(-E_a/k_B T)} + b \times exp^{(-E_b/k_B T)}}, \quad (3)$$

where I_0 is the low temperature PL intensity. The activation energies E_b is associated to exciton binding energy, E_a is the self-trapped depth ($E_a = E_{FE} - E_{STE}$), E_c describe the thermal quenching of the PL intensity, and a, b and c are fitting parameters. The best refinement gives E_a = 25 ± 0.8 meV, E_b = 138 ± 5 meV, and E_c = 5.9 ± 0.4 meV for $CsCu_2Cl_{1.5}Br_{1.5}$ and E_a = 29 ± 5 (3) meV, E_b = 98 ± 8 meV, and E_c = 12.2 ± 0.7 meV for $CsCu_2Br_{1.5}I_{1.5}$. Note that the obtained E_a values are close to the RT thermal energy (~ 26 meV), so it would be reasonable to expect the free excitonic emission at RT. However, the absence of the free exciton peaks is probably due to the very broad

STEs emission band compared to free-exciton emission. This also confirms the intrinsic nature of the trapping mechanism.[25-26, 44]

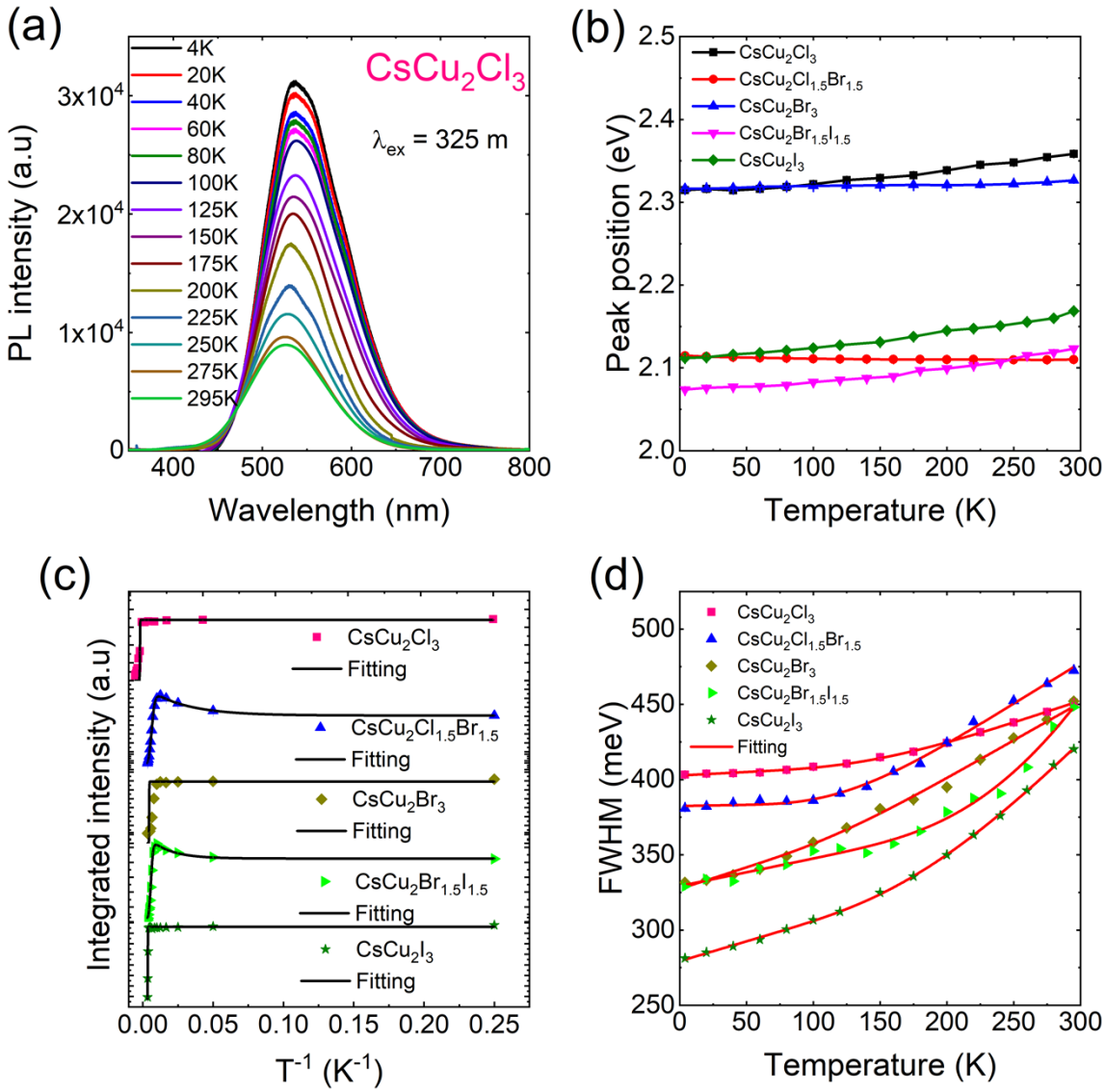

Figure 4. (a) Temperature-dependent PL spectra of $CsCu_2Cl_3$, under 325 nm excitation. Thermal evolution of (b) position, (c) integrated intensity, and (d) FHWM of PL peaks of $CsCu_2X_3$. The integrated PL intensity were refined (black curves) based on Eqs (2-3). FWHM were refined based on Eq (4) (red curves).

Moreover, the thermal broadening in linewidth of PL of $CsCu_2X_3$ (Figure 4c) originates from exciton-phonon coupling, and described by,

$$\Gamma(\mathrm{T}) = \Gamma_0 + \Gamma_{\mathrm{AC}} \times T + \Gamma_{\mathrm{LO}} \times \left(1 + exp\left(\frac{E_{\mathrm{LO}}}{k_{\mathrm{B}}T}\right)\right)^{-1}, \qquad (4)$$

where the first term is the natural line width at 0 K, the second term represents the broadening induced by acoustic phonons, and the third term corresponds to the contribution of optical phonons to the peak broadening. There, Γ_{LO} is the exciton-phonon coupling constant and E_{LO} is the optical phonon energy. The fitting gives Γ_{LO} and E_{LO} values ranging from 471 to 910 meV K^{-1} and from 4.1 to 12.2 meV, respectively. These high exciton-phonon coupling constant values are one order of magnitude larger than those of lead-based 3D hybrid perovskites (Γ_{LO} of 40-61 meV)[45] and more than two times higher than the reported value of $Cs_3Bi_2I_6Cl_3$,[9] supporting the strength of the electron-phonon coupling in $CsCu_2X_3$. Moreover, E_{LO} values of 6.2 and 11.5 meV for $CsCu_2Cl_{1.5}Br_{1.5}$ and $CsCu_2Cl_{1.5}Br_{1.5}$, respectively, are in excellent agreement with the E_c values of 5.9 ± 0.4 meV and 12.2 ± 0.7 meV deduced from the fitting of the PL intensity using Shibata's model. Together, these findings support the assignment of the broad PL emission of $CsCu_2X_3$ to phonon-assisted recombination of STEs.

Finally, we also carried out preliminary attempts to make LEDs based on $CsCu_2X_3$ (see Figure S11). In order to fabricate LEDs, a $CsCu_2I_3$ was used as a yellow additive in an 1,3-Bis(N-carbazolyl)benzene (mCP) host layer (see SI for more details) . The $CsCu_2I_3$-based LED shows a yellow emission light with the peak wavelength of 554nm. The quantum efficiency of ~ 0.1 % was achieved at the luminance of 1 cd/m^2. Further optimization efforts are currently ongoing and will be reported in a forthcoming paper.

In conclusion, we report the optical properties of nontoxic, remarkably stable, and highly emissive 1D metal halides $CsCu_2X_3$ (X = Cl, Br, I). Bright RT visible-emission was found with PLQY reaching 48% for $CsCu_2Cl_3$, attributed to STEs. The photophysical properties of $CsCu_2X_3$ were investigated through temperature, power dependence and time resolved PL measurements.

High exciton binding energies ranging from 98 to 201 meV and high exciton-phonon coupling energies were estimated from the thermal evolution of PL intensity and FWHM. Our findings support the assignment of the broad PL emission of $CsCu_2X_3$ to phonon-assisted recombination of STEs. Importantly, this work demonstrates the development of all-inorganic Pb-free halide light emitters $CsCu_2X_3$, a which constitutes a significant advancement in the development of future solid-state lighting technologies based on inexpensive, nontoxic and earth-abundant materials.

ASSOCIATED CONTENT

Supporting Information

The Supporting Information is available free of charge on the ACS Publications website.

Experimental details, tables with interatomic distances and bond angles, distortion calculations, and refinement details of time-resolved and temperature dependence photoluminescence, powder X-ray diffraction patterns, DSC/TGA, diffuse reflectance, temperature and power dependence photoluminescence full data, and quantum efficiency of the fabricated device.

AUTHORS INFORMATION.

Corresponding Author

*E-mail: saparov@ou.edu

Authors Contribution

This manuscript was written through contribution of all authors. All authors have given approval to the final version of the manuscript. R. R. prepared the samples, performed XRD and room temperature optical measurements, A. Y. carried out power- and temperature-dependent PL measurements and analyzed the data, Y. W. measured the time-resolved PL data, T. C. carried out photosensitivity studies, G. S. and D.-Y. K. performed device preparation and measurements, M.-

H. D. performed density functional theory calculations, and B. S. conceived and supervised the work. All authors contributed to the writing of the writing of this paper.

Notes

The authors declare no competing financial interests.

ACKNOWLEDGMENTS.

This work was supported by the University of Oklahoma (OU) startup funds and support from the College of Arts and Sciences at OU. A. Y. acknowledges Dr. Vincent R. Whiteside and Dr. Ian R. Sellers for technical assistance with photoluminescence measurements. M. -H. Du was supported by the U. S. Department of Energy, Office of Science, Basic Energy Sciences, Materials Sciences and Engineering Division.

REFERENCES

1. Zhou, C.; Tian, Y.; Yuan, Z.; Lin, H.; Chen, B.; Clark, R.; Dilbeck, T.; Zhou, Y.; Hurley, J.; Neu, J.; Besara, T.; Siegrist, T.; Djurovich, P.; Ma, B., Highly Efficient Broadband Yellow Phosphor Based on Zero-Dimensional Tin Mixed-Halide Perovskite. *ACS Appl. Mater. Interfaces.* **2017,** *9* (51), 44579-44583.
2. Kim, Y.-H.; Cho, H.; Lee, T.-W., Metal halide perovskite light emitters. *Proc. Nat. Acad. Sci.* **2016,** *113* (42), 11694-11702.
3. Tan, Z.-K.; Moghaddam, R. S.; Lai, M. L.; Docampo, P.; Higler, R.; Deschler, F.; Price, M.; Sadhanala, A.; Pazos, L. M.; Credgington, D.; *et al.*, Bright light-emitting diodes based on organometal halide perovskite. *Nat. Nanotechnol.* **2014,** *9*, 687.
4. Yangui, A.; Pillet, S.; Garrot, D.; Triki, S.; Abid, Y.; Boukheddaden, K., Evidence and detailed study of a second-order phase transition in the $(C_6H_{11}NH_3)_2[PbI_4]$ organic-inorganic hybrid material. *J. Appl. Phys.* **2015,** *117* (11), 115503: 1-9.
5. Pathak, S.; Sakai, N.; Wisnivesky Rocca Rivarola, F.; Stranks, S. D.; Liu, J.; Eperon, G. E.; Ducati, C.; Wojciechowski, K.; Griffiths, J. T.; Haghighirad, A. A.; Pellaroque, A.; *et al.*, Perovskite Crystals for Tunable White Light Emission. *Chem. Mater.* **2015,** *27* (23), 8066-8075.
6. Protesescu, L.; Yakunin, S.; Bodnarchuk, M. I.; Krieg, F.; Caputo, R.; Hendon, C. H.; Yang, R. X.; Walsh, A.; Kovalenko, M. V., Nanocrystals of Cesium Lead Halide Perovskites ($CsPbX_3$, X = Cl, Br, and I): Novel Optoelectronic Materials Showing Bright Emission with Wide Color Gamut. *Nano Lett.* **2015,** *15* (6), 3692-3696.
7. Yang, H.; Zhang, Y.; Pan, J.; Yin, J.; Bakr, O. M.; Mohammed, O. F., Room-temperature engineering of all-inorganic perovskite nanocrsytals with different dimensionalities. *Chem. Mater.* **2017,** *29* (21), 8978-8982.
8. Saparov, B.; Mitzi, D. B., Organic–Inorganic Perovskites: Structural Versatility for Functional Materials Design. *Chem. Rev.* **2016,** *116*, 4558-4596.

9. McCall, K. M.; Stoumpos, C. C.; Kontsevoi, O. Y.; Alexander, G. C. B.; Wessels, B. W.; Kanatzidis, M. G., From 0D $Cs_3Bi_2I_9$ to 2D $Cs_3Bi_2I_6Cl_3$: Dimensional Expansion Induces a Direct Band Gap but Enhances Electron–Phonon Coupling. *Chem. Mater.* **2019**. *31* (7), 2644-2650.
10. Saidaminov, M. I.; Almutlaq, J.; Sarmah, S.; Dursun, I.; Zhumekenov, A. A.; Begum, R.; Pan, J.; Cho, N.; Mohammed, O. F.; Bakr, O. M., Pure Cs_4PbBr_6: Highly Luminescent Zero-Dimensional Perovskite Solids. *ACS Energy Lett.* **2016,** *1* (4), 840-845.
11. Li, T.; Mo, X.; Peng, C.; Lu, Q.; Qi, C.; Tao, X.; Ouyang, Y.; Zhou, Y., Distinct green electroluminescence from lead-free $CsCuBr_2$ halide micro-crosses. *Chem. Commun.* **2019**. *55*, 4554-4557.
12. Booker, E. P.; Griffiths, J. T.; Eyre, L.; Ducati, C.; Greenham, N. C.; Davis, N. J. L. K., Synthesis, Characterization, and Morphological Control of Cs_2CuCl_4 Nanocrystals. *J. Phys. Chem. C* **2019,** *123* (27), 16951-16956.
13. Roccanova, R.; Yangui, A.; Nhalil, H.; Shi, H.; Du, M.-H.; Saparov, B., Near-Unity Photoluminescence Quantum Yield in Blue-Emitting $Cs_3Cu_2Br_{5-x}I_x$ ($0 \leq x \leq 5$). *ACS Appl. Electron. Mater.* **2019,** *1* (3), 269–274.
14. Association, O. I. D., The Promise of Solid State Lighting for General Illumination. Washington, DC: US Department of Energy, Office of Energy Efficiency and …: 2001.
15. Meyer, G., Synproportionierung am metallischen Substrat: $CsCu_2Cl_3$ und $CsCu_2Br_3$. *Z. Anorg. Allg. Chem.* **1984,** *515* (8), 127-132.
16. Jouini, N.; Guen, L.; Tournoux, M., Structure cristalline de $CsCu2I_3$. *Rev. Chim. Mineral* **1980,** *17*, 486-491.
17. Zhang, X.; Liu, H.; Wang, W.; Zhang, J.; Xu, B.; Karen, K. L.; Zheng, Y.; Liu, S.; Chen, S.; Wang, K., Hybrid Perovskite Light-Emitting Diodes Based on Perovskite Nanocrystals with Organic–Inorganic Mixed Cations. *Adv. Mater.* **2017,** *29* (18), 1606405.
18. Leijtens, T.; Prasanna, R.; Gold-Parker, A.; Toney, M. F.; McGehee, M. D., Mechanism of Tin Oxidation and Stabilization by Lead Substitution in Tin Halide Perovskites. *ACS Energy Letters* **2017,** *2* (9), 2159-2165.
19. Wojakowska, A.; Krzyżak, E.; Wojakowski, A., Phase diagram for the CuBr–CsBr system. *Thermochim. Acta* **2000,** *344* (1-2), 55-59.
20. Wojakowska, A.; Gorniak, A.; Kuznetsov, A. Y.; Wojakowski, A.; Josiak, J., Phase diagram of the system copper (I) iodide+ cesium iodide. *J.Chem. Eng. Data.* **2003,** *48* (3), 468-471.
21. Kawai, T.; Ishii, A.; Kitamura, T.; Shimanuki, S.; Iwata, M.; Ishibashi, Y., Optical Absorption in Band-Edge Region of $(CH_3NH_3)_3Bi_2I_9$ Single Crystals. *J. Phys. Soc. Jpn.* **1996,** *65* (5), 1464-1468.
22. Lin, H.; Zhou, C.; Tian, Y.; Siegrist, T.; Ma, B., Low-Dimensional Organometal Halide Perovskites. *ACS Energy Lett.* **2018,** *3* (1), 54-62.
23. Zhang, R.; Mao, X.; Yang, Y.; Yang, S.; Zhao, W.; Wumaier, T.; Wei, D.; Deng, W.; Han, K., Air-Stable, Lead-Free Zero-Dimensional Mixed Bismuth-Antimony Perovskite Single Crystals with Ultra-broadband Emission. *Angew. Chem.* **2019,** *131* (9), 2751-2755.
24. Bowers, M. J.; McBride, J. R.; Rosenthal, S. J., White-Light Emission from Magic-Sized Cadmium Selenide Nanocrystals. *J. Am. Chem. Soc.* **2005,** *127* (44), 15378-15379.
25. Yangui, A.; Garrot, D.; Lauret, J. S.; Lusson, A.; Bouchez, G.; Deleporte, E.; Pillet, S.; Bendeif, E. E.; Castro, M.; Triki, S.; Abid, Y.; Boukheddaden, K., Optical Investigation of Broadband White-Light Emission in Self-Assembled Organic–Inorganic Perovskite $(C_6H_{11}NH_3)2PbBr_4$. *J. Phys. Chem. C* **2015,** *119* (41), 23638-23647.

26. Smith, M. D.; Karunadasa, H. I., White-Light Emission from Layered Halide Perovskites. *Acc. Chem. Res.* **2018,** *51* (3), 619-627.
27. Yin, W.-J.; Yan, Y.; Wei, S.-H., Anomalous Alloy Properties in Mixed Halide Perovskites. *J. Phys. Chem. Lett.* **2014,** *5* (21), 3625-3631.
28. Yangui, A.; Pillet, S.; Lusson, A.; Bendeif, E. E.; Triki, S.; Abid, Y.; Boukheddaden, K., Control of the White-Light Emission in the Mixed Two-Dimensional Hybrid Perovskites $(C_6H_{11}NH_3)_2[PbBr_{4-x}I_x]$. *J. Alloys Compd.* **2017,** *699*, 1122-1133.
29. Aneesh, J.; Swarnkar, A.; Kumar Ravi, V.; Sharma, R.; Nag, A.; Adarsh, K. V., Ultrafast Exciton Dynamics in Colloidal CsPbBr3 Perovskite Nanocrystals: Biexciton Effect and Auger Recombination. *J. Phys. Chem. C.* **2017,** *121* (8), 4734-4739.
30. Mott, N. F.; Stoneham, A. M., The lifetime of electrons, holes and excitons before self-trapping. *J. Phys. C: Solid St. Phys.* **1977,** *10* (17), 3391-3398.
31. Varshni, Y., Temperature dependence of the energy gap in semiconductors. *Physica.* **1967,** *34* (1), 149-154.
32. Yangui, A.; Pillet, S.; Bendeif, E.-E.; Lusson, A.; Triki, S.; Abid, Y.; Boukheddaden, K., Broadband Emission in a New Two-Dimensional Cd-Based Hybrid Perovskite. *ACS Photonics.* **2018,** *5* (4), 1599-1611.
33. Li, J.; Yuan, X.; Jing, P.; Li, J.; Wei, M.; Hua, J.; Zhao, J.; Tian, L., Temperature-dependent photoluminescence of inorganic perovskite nanocrystal films. *RSC Adv.* **2016,** *6* (82), 78311-78316.
34. Gaponenko, M. S.; Lutich, A. A.; Tolstik, N. A.; Onushchenko, A. A.; Malyarevich, A. M.; Petrov, E. P.; Yumashev, K. V., Temperature-dependent photoluminescence of PbS quantum dots in glass: Evidence of exciton state splitting and carrier trapping. *Phys. Rev. B.* **2010,** *82* (12), 125320.
35. Hong, X.; Ishihara, T.; Nurmikko, A., Dielectric confinement effect on excitons in PbI4-based layered semiconductors. *Phys. Rev. B.* **1992,** *45* (12), 6961-6964.
36. Yang, H.; Zhang, Y.; Pan, J.; Yin, J.; Bakr, O. M.; Mohammed, O. F., Room-Temperature Engineering of All-Inorganic Perovskite Nanocrsytals with Different Dimensionalities. *Chem. Mater.* **2017,** *29* (21), 8978-8982.
37. Li, F.; Yang, L.; Cai, Z.; Wei, K.; Lin, F.; You, J.; Jiang, T.; Wang, Y.; Chen, X., Enhancing exciton binding energy and photoluminescence of formamidinium lead bromide by reducing its dimensions to 2D nanoplates for producing efficient light emitting diodes. *Nanoscale* **2018,** *10* (44), 20611-20617.
38. Longo, G.; La-Placa, M.-G.; Sessolo, M.; Bolink, H. J., High Photoluminescence Quantum Yields in Organic Semiconductor–Perovskite Composite Thin Films. *ChemSusChem.* **2017,** *10* (19), 3788-3793.
39. Droseros, N.; Longo, G.; Brauer, J. C.; Sessolo, M.; Bolink, H. J.; Banerji, N., Origin of the Enhanced Photoluminescence Quantum Yield in MAPbBr3 Perovskite with Reduced Crystal Size. *ACS Energy Lett.* **2018,** *3* (6), 1458-1466.
40. Shibata, H., Negative Thermal Quenching Curves in Photoluminescence of Solids. *Jpn. J. Appl. Phys.* **1998,** *37* (Part 1, No. 2), 550-553.
41. Wu, Y.; Li, J.; Ding, H.; Gao, Z.; Wu, Y.; Pan, N.; Wang, X., Negative thermal quenching of photoluminescence in annealed ZnO–Al2O3 core–shell nanorods. *Phys. Chem. Chem. Phys.* **2015,** *17* (7), 5360-5365.

42. Ling, Y.; Tan, L.; Wang, X.; Zhou, Y.; Xin, Y.; Ma, B.; Hanson, K.; Gao, H., Composite Perovskites of Cesium Lead Bromide for Optimized Photoluminescence. *J. Phys. Chem. Lett.* **2017,** *8* (14), 3266-3271.
43. Smith, M. D.; Jaffe, A.; Dohner, E. R.; Lindenberg, A. M.; Karunadasa, H. I., Structural Origins of Broadband Emission from Layered Pb–Br Hybrid Perovskites. *Chem. Sci.* **2017,** *8*, 4497-4504.
44. McCall, K. M.; Stoumpos, C. C.; Kostina, S. S.; Kanatzidis, M. G.; Wessels, B. W., Strong Electron–Phonon Coupling and Self-Trapped Excitons in the Defect Halide Perovskites $A_3M_2I_9$ (A = Cs, Rb; M = Bi, Sb). *Chem. Mater.* **2017,** *29* (9), 4129-4145.
45. Wright, A. D.; Verdi, C.; Milot, R. L.; Eperon, G. E.; Pérez-Osorio, M. A.; Snaith, H. J.; Giustino, F.; Johnston, M. B.; Herz, L. M., Electron–phonon coupling in hybrid lead halide perovskites. *Nat. Commun.* **2016,** *7*, 11755.